The Mechanism of Proton Transfer between Adjacent Sites Exposed to Water

Aviv Mezer,† Ran Friedman,† Orly Noivirt, Esther Nachliel, and Menachem Gutman*

Laser Laboratory for Fast Reactions in Biology, Department of Biochemistry, George S. Wise Faculty of Life Sciences, Tel Aviv University, Israel

Received: August 22, 2004; In Final Form: March 24, 2005

The surface of a protein, or a membrane, is spotted with a multitude of proton-binding sites, some of which are only a few angstroms apart. When a proton is released from one site, it propagates through the water by a random walk under the bias of the local electrostatic potential determined by the distribution of the charges on the protein. Some of the released protons disperse into the bulk, but during the first few nanoseconds, the released protons can be trapped by encounter with nearby acceptor sites. This process resembles a scenario which corresponds with the time-dependent Debye−Smoluchowski equation. In the present study, we investigated the mechanism of proton transfer between sites that are only a few angstroms apart, using as a model the proton exchange between sites on a small molecule, fluorescein, having two, spectrally distinguishable, proton-binding sites. The first site is the oxyanion on the chromophore ring structure. The second site is the carboxylate moiety on the benzene ring of the molecule. Through our experiments, we were able to reconstruct the state of protonation at each site and the velocity of proton transfer between them. The fluorescein was protonated by a few nanosecond long proton pulse under specific conditions that ensured that the dye molecules would be protonated only by a single proton. The dynamics of the protonation of the chromophore were measured under varying initial conditions (temperature, ionic strength, and different solvents (H_2O or D_2O)), and the velocity of the proton transfer between the two sites was extracted from the overall global analysis of the signals. The dynamics of the proton transfer between the two proton-binding sites of the fluorescein indicated that the efficiency of the site-to-site proton transfer is very sensitive to the presence of the screening electrolyte and has a very high kinetic isotope effect (KIE = 55). These two parameters clearly distinguish the mechanism from proton diffusion in bulk water. The activation energy of the reaction (E_a = 11 kcal mol^{-1}) is also significantly higher than the activation energy for proton dissociation in bulk water ($E_a \sim 2.5$ kcal mol^{-1}). These observations are discussed with respect to the effect of the solute on the water molecules located within the solvation layer.

Introduction

Proton-transfer reactions are the most common biochemical reactions; as in almost any enzymatic catalysis, a proton is consumed, is produced, or serves as an intermediate. High turnover proton-pumping proteins, such as cytochrome oxidase,[1−3] photosynthetic reaction center,[2,3] or Bacteriorhodopsin,[4] have developed efficient proton-collecting antenna systems on their surfaces. These systems utilize clusters of carboxylates (proton attractor sites) and histidine residues (acting as a local proton reservoir) which alleviate the necessity for an encounter between the active site and the free proton (for a review, see ref 5). The mechanism of proton transfer common to these systems consists of donor−acceptor pairs, each located at a distance of a few angstroms from the other, which exchange protons among themselves through interspaced water molecules. The special features of these systems are the proximity between the sites and the fact that the water molecules interact with the matrix to which the proton-binding sites are attached. The distance between the reacting residues is in the order of their Coulomb cage radii. The reactions proceed through the water molecules inside the Coulomb cage, where the solvent−solute interactions arrange the water through charge−dipole and dipole−dipole interactions. The local ordering of the water can affect their capacity to support proton-transfer reactions.

The excess proton in water has two stable forms, $H_9O_4^+$ and $H_5O_2^+$, that are in rapid equilibrium with each other. In $H_9O_4^+$, the proton is tightly bound to a water molecule, which maintains strong hydrogen bonds with three other water molecules. The distance between two oxygen atoms of this structure is only 2.54 Å, significantly shorter than the average (2.8 Å) O−O in water. This structure is stabilized by its second solvation shell[6,7] which shares 30% of the protonic charge. The $H_5O_2^+$ complex is a proton shared by two water molecules. Each flanking molecule forms four hydrogen bonds, one with the proton and three with the surrounding solvent. The transition between the two configurations is initiated through the random motion of water molecules in the second solvation shell of the charged complexes.[8] Once the solvent assumes a favorable structure, there is a reshuffling of the electronic configuration in the complex, shifting the extra charge of the proton (but not its mass) from one water molecule to the other. During the proton-transfer step, there is a shortening of the hydrogen-bond length in the first and second solvation shells.[8] This special mechanism translocates the protonic charge but not its mass, acquiring proton (and the hydroxyl anion) with a diffusion coefficient larger than any other ion in aqueous solution.[6,7,9−12] At a molecular level, the rate-limiting step of proton transfer in solution is the organization of the surrounding solvent mol-

* To whom correspondence should be addressed. E-mail: me@hemi.tau.ac.il.

† These authors made an equal contribution to this study.

10.1021/jp046213i CCC: $30.25
Published on Web 05/12/2005

CHART 1. The Fluorescein Molecule

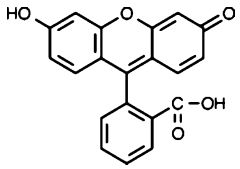

ecules.[8] This step can be considered as a motion along the solvent coordinate in order to generate a transition state where the proton can move, in an equipotential manner, from the donor to the acceptor site. The actual proton transfer within the transition state is almost barrierless.[13,14] The reorganization energy of the water molecules in the second solvation shell sets the activation energy of the process ($\sim$2.5 kcal mol^{-1},[7] and the magnitude of the kinetic isotope effect $\sim\sqrt{2}$[11]). Under conditions where the distance between the heavy atoms is extended, the activation energy increases above the reorganization energy and a new regime is established, where the proton transfer is the rate-limiting step,[15−17] and the kinetic isotope effect of the proton transfer can increase to very high values.[18]

Proton transfer between adjacent sites on the surface of a protein occurs inside the Coulomb cage, which surrounds two nearby proton-binding sites. In this special environment, the relative motion of the water molecules (and hence the reorganization energy) is determined not only by the stability of the hydrogen bonds between the water molecules but also by their interactions with the charges and the dipoles of the protein. Thus, we can expect to find a larger activation energy and kinetic isotope effect for proton transfer near a protein.

The dynamics of proton transfer between sites on proteins or other molecules can be followed using methods which utilize a laser pulse to synchronize the excitation of photoacid compounds. In the excited state, these compounds redistribute the electrons in molecular orbitals, initiating proton translocation events. The experimental observation consists of a continuous follow-up of the fluorescence of the excited molecule, with a picosecond time resolution. Many studies were carried out either in aprotic solvents or when the system was supplemented with a limited number of water molecules that provided the proton transport pathway.[19−33] However, these studies differ from proton-transfer reactions between sites located inside a common Coulomb cage on the surface of a well solvated enzyme, a situation common to all proton-pumping proteins that have to pick up a proton from the bulk and deliver it to the orifice of their proton-conducting channel.[34]

Ideally, the best system for studying the proton transfer at the surface of a macromolecule will be based on a model protein and will couple the measurements with molecular modeling calculations. On the other hand, only a small fraction of the protein's surface participates in the proton-transfer reactions; thus, a small model molecule can provide a simpler system for study, with the advantage that advanced molecular modeling procedures can be performed. For this reason, we decided to study the intramolecular proton transfer with the fluorescein molecule as a model.

The fluorescein (see Chart 1) is a commonly used pH indicator that has two proton-binding sites. The familiar proton-binding site of the dye is the oxyanion attached to the xanthene ring. In the present text, we shall refer to this section of the dye as the chromophore and mark it by **Flu**$^-$. Protonation of the oxyanion (pK = 6.6) leads to an instantaneous shift of the absorbance maximum, from 496 to 460 nm, with an appreciable decrease in the extinction coefficient. The second proton-binding site of fluorescein is the carboxylate on the benzene ring (marked in the present text as **COO**$^-$, pK = 5.2). The protonation of the **COO**$^-$ has a delayed effect on the dye's spectrum; once the carboxylate is protonated, the molecule undergoes a slow tautomerization, closing a lactam ring. This form has no absorption in the visible. Yet, as the tautomer formation has a time constant (τ > 10 ms) that is much longer than our observation time (100−300 μs), this reaction is neither observed nor considered in our calculations. In this study, we measured the dynamics of proton transfer from the carboxylate of the fluorescein to the oxyanion of the chromophore. Since the pK of the carboxylate is lower than that of the oxyanion, the reaction is practically unidirectional. The distance between the donor and the oxyanion is too large to allow proton transfer without the involvement of water molecules. The proton should first be released from the carboxylic moiety, creating a fluorescein dianion. Later, the solvated proton has to propagate through the water before it can react with the acceptor to form the covalent bond.[35] This pathway is in competition with a parallel path leading to the escape of the proton to the bulk. The two pathways differ in some basic features; the latter is driven by the entropy of dispersion, but the proton has to overcome the potential barrier posed by the Coulomb cage, while the first is limited in length and consists of very few water molecules connecting between the donor and acceptor atoms.

The protonation of fluorescein can be synchronized by the laser induced proton pulse (LIPP) technique. The indicator is dissolved in a dilute aqueous solution of pyranine, which is a dye that, upon excitation, lowers its pK and releases a proton within 100 ps. Thus, pulse irradiation of the solution drives a temporary acid−base disequilibrium.[36,37] The protons released from the excited pyranine react in a diffusion-controlled reaction with the ground state pyranine anion and the fluorescein, where the rates of protonation of both the oxyanion and the carboxylate are approximately the same. The system relaxes to the prepulse state by multiple pathways, where the proton transfer from the carboxylate to the oxyanion is one of the reactions. The whole relaxation dynamics are subjected to a rigorous kinetic analysis, where all reactions are transformed into a set of coupled, nonlinear differential rate equations that replicate all chemical processes which take place in the reaction space. The integration of these equations, with the proper rate constants, can reconstruct the observed signal. In the present study, we employed this methodology to determine the rate constants of all proton-transfer reactions which characterize the overall process and include the intramolecular process.

The present study demonstrates that the proton transfer between the distinct sites of the fluorescein molecule consists of two parallel pathways. Both pathways are initiated by a common rate-limiting step, the release of the proton from the carboxylic moiety of the benzene ring. The released proton can either diffuse to the bulk or, while it executes its random walk inside the Coulomb cage, react with the oxyanion on the chromophore ring structure. The efficiency of the latter pathway is as high as $\sim$50% and differs from the diffusion in bulk water by three major features: high activation energy (11 kcal mol^{-1}), extremely high kinetic isotope effect (KIE = 55), and high sensitivity to screening electrolytes. These observations demonstrate that the water molecules within the inner solvation layer of charged bodies are strongly affected by the solute, leading to a different regime of proton-transfer dynamics.

Materials and Methods

Materials. Pyranine (8-hydroxy-pyrene-1,3,6-trisulfonate, laser grade), fluorescein, and D_2O were obtained from Sigma.

Kinetic Measurements. The kinetic measurements were carried out in a solution containing pyranine (5−15 μM) and fluorescein (5−15 μM), either in pure water or D_2O (98% D_2O in the reaction mixture). The pH of the solution was adjusted by the addition of small aliquots of either HCl or NaOH (10 mM each), and the pH was continuously monitored during the reaction time.

The solution was irradiated by a train of short laser pulses (3 ns fwhm) with an energy of 1.5−2.1 mJ, each at a frequency of 10 Hz. At this energy level, the concentration of the protons released from reaction-excited pyranine molecules is only 2−3 μM, which is smaller than the number of available proton-binding sites (pyranine anion plus the ionized carboxylate and oxyanion present in the solution). This ensures that the probability of double protonation of the fluorescein is negligible.

The transient absorbencies of the irradiated solution were monitored by a Tektronix TDS 520A 500 MHz digital oscilloscope which has a time resolution of 50 ns. The jitter time of the triggering system was less than 5 ns, and signals were averaged without broadening of the time resolution.

The transient absorbencies of the pyranine ($\mathbf{\Phi O^-}$) and the fluorescein ($\mathbf{Flu^-}$) were monitored at 458 and 496 nm, respectively ($\epsilon_{\text{pyranine(458nm)}} = 24\,000\ M^{-1}\ cm^{-1}$; $\epsilon_{\text{fluorescein(496nm)}} = 63\,000\ M^{-1}\ cm^{-1}$). The signals were recorded by Tektronix 520A oscilloscope and a computer program that removed the digitization limits of the oscilloscope. For more technical details, see refs 36−38. The third proton-binding site present in the system is the carboxylate moiety of the fluorescein. Due to the fact that the free proton concentration in the reaction mixture relaxes to the prepulse level within 1−2 μs,[38−40] the state of protonation of the carboxylate can be quantitated at any time as the difference between two measured parameters: $[\mathbf{COOH}]_t = [\mathbf{\Phi O^-}]_t - [\mathbf{Flu^-}]_t$. Thus, the reconstruction of the dynamics can be carried out with full account for any proton in the system.

Kinetic Analysis of the Absorbance Transients. The analysis of the measured signals is based on numeric integration of differential rate equations that account for any proton-transfer reaction among the proton-binding sites present in the reaction system. Thus, in the pyranine−fluorescein system, there are six proton-transfer reactions:

$$1.\ \mathbf{\Phi O^-} + \mathbf{H^+} \leftrightarrow \mathbf{\Phi OH}$$

$$2.\ \mathbf{FLU^-} + \mathbf{H^+} \leftrightarrow \mathbf{FLUH}$$

$$3.\ \mathbf{COO^-} + \mathbf{H^+} \leftrightarrow \mathbf{COOH}$$

$$4.\ \mathbf{FLUH} + \mathbf{\Phi O^-} \leftrightarrow \mathbf{FLU^-} + \mathbf{\Phi OH}$$

$$5.\ \mathbf{COOH} + \mathbf{\Phi O^-} \leftrightarrow \mathbf{COO^-} + \mathbf{\Phi OH}$$

$$6.\ \mathbf{COOH} + \mathbf{FLU^-} \leftrightarrow \mathbf{COO^-} + \mathbf{FLUH}$$

Reactions 1−3 correspond with the diffusion-controlled reaction between a free proton and acceptor, and the rate constants are compatible with the values predicted by the Debye−Smoluchowski equation for diffusion-controlled reactions.[5,41−44] It should be stressed that reactions 2 and 3 represent the encounter of a free-diffusing proton with the outer perimeter of the fluorescein's Coulomb cage ($r = 14$ Å for the dianion state). A proton that encounters the Coulomb cage will be taken up by the dye with an equal probability to form a covalent bond with either the oxyanion or the carboxylate. For this reason, the rate constants of reactions 2 and 3 were set during the search to be equal.

Reactions 4 and 5 describe a collisional proton transfer between two free-diffusing reactants, and the rate constants are also compatible with the theoretical predictions.[5,41−44] Reaction 6 differs from the two other collisional proton-transfer reactions, as it represents either a proton transfer between two fluorescein molecules or an intramolecular one.

The whole system was converted into a set of coupled, nonlinear differential rate equations that are consistent with the microscopic reversibility, mass action, and mass conservation laws. The numeric integration of these equations, using the experimental concentrations as constants and the reaction rate constants as adjustable parameters, can reconstruct the observed signals with high accuracy.

The kinetic experiments were repeated under varying initial pHs and reactant concentrations, and all signals were reconstructed by the integration of the differential rate equations using the rate constants as adjustable parameters. A solution was considered as acceptable when some 10−15 independent measurements were reconstructed by a single set of parameters, each varying within a range of 20% or less.

The activation energy was determined by repeating the measurement at varying temperatures. However, as the analysis is aimed for the best reconstruction of the observed signals, the spread of the rate constants from the linear correlation was, in some cases, as large as 50%.

Molecular Dynamics Simulation of Fluorescein in the Oxyanion State. The starting structure of the fluorescein molecule was modeled using the computer program GAMESS,[45] using density functional theory (DFT) with the 6-31G* basis set. The density functionals were calculated using the B3LYP functional.[46−48] The molecule was then put into a truncated, octahedral shaped box containing TIP3P model water,[49] leaving at least 1 nm between the solute and the edge of the box. One of the water molecules (selected randomly) was replaced by a sodium ion to keep the system neutral, leaving a total of 639 water molecules. Then, a brief energy minimization took place using the GROMACS 3.2.1 simulation package[50] and the OPLS force field.[51−54] The system was equilibrated by first running 20 ps of position restrained molecular dynamics and 50 ps of unrestrained molecular dynamics, before performing an MD run of 500 ps. The structures of the fluorescein and all water molecules were saved for further processing at 0.5 ps intervals. Both minimization and the molecular dynamics were carried out with the GROMACS 3.2.1 program.

The OPLS force field parameters for the fluorescein were set as follows. The partial charges were determined by fitting them to the electrostatic potential around the molecule using the Kollman−Singh method.[55] OPLS atom types were set for each fluorescein atom, using the closest atom type as featured in the GROMACS package. The partial charges and the atom types are given in the Supporting Information. The program pdb2gmx, which is part of the GROMACS package, was used to set the list of constraints for bonds, angles, and dihedrals. In cases where the program was unable to assign appropriate values, these were added manually by selecting the appropriate terms from the OPLS force field as implemented in GROMACS. A similar approach was used for setting the atom types in the PRODRG server for usage of small molecules in GROMACS.[56]

Two additional MD simulation runs, involving a hydronium ion which is treated classically, were set as follows. In the first simulation, one of the water molecules located in the proposed proton-transfer pathway between the fluorescein donor and acceptor (see Figure 4) was replaced by hydronium. The system was energy-minimized as described above. Then, three subse-

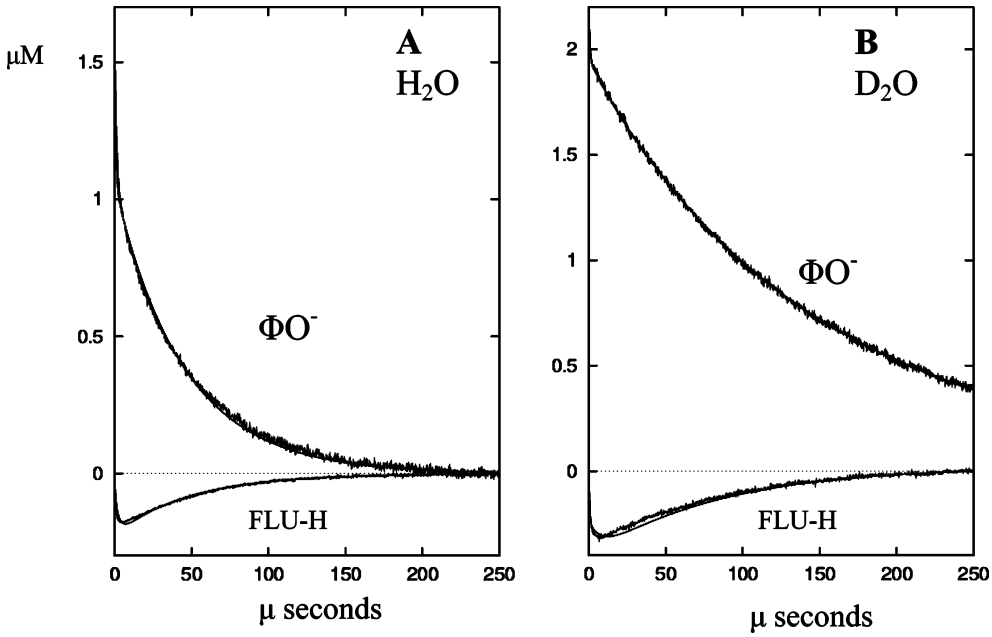

Figure 1. Proton-transfer dynamics between pyranine and fluorescein in neat water (A) and in D_2O (98%) (B). The reactions were measured in the presence of pyranine (19.7 and 21.3 μM for frames A and B, respectively) and fluorescein (12.4 and 14.28 μM) at pH 7.1 and 7.04 (for frames A and B, respectively). The temperatures of the measurements were 20.8 °C (A) and 22.8 °C (B). Each signal is an average of 1000 events. The top curve in each frame depicts the reprotonation of the $\mathbf{\Phi O}^-$ anion generated by the laser pulse, measured as the incremental absorbance at 458 nm. The lower curve in each frame corresponds with the reversible protonation of fluorescein, measured as a bleaching of the fluorescein absorbance at 496 nm. The transients were converted to molar units after correction for the precise absorption spectrum of the dyes. The continuous lines are the reconstruction of the dynamics by integration of differential rate equations describing a delta function perturbation of the reactions given by eqs 1−6.

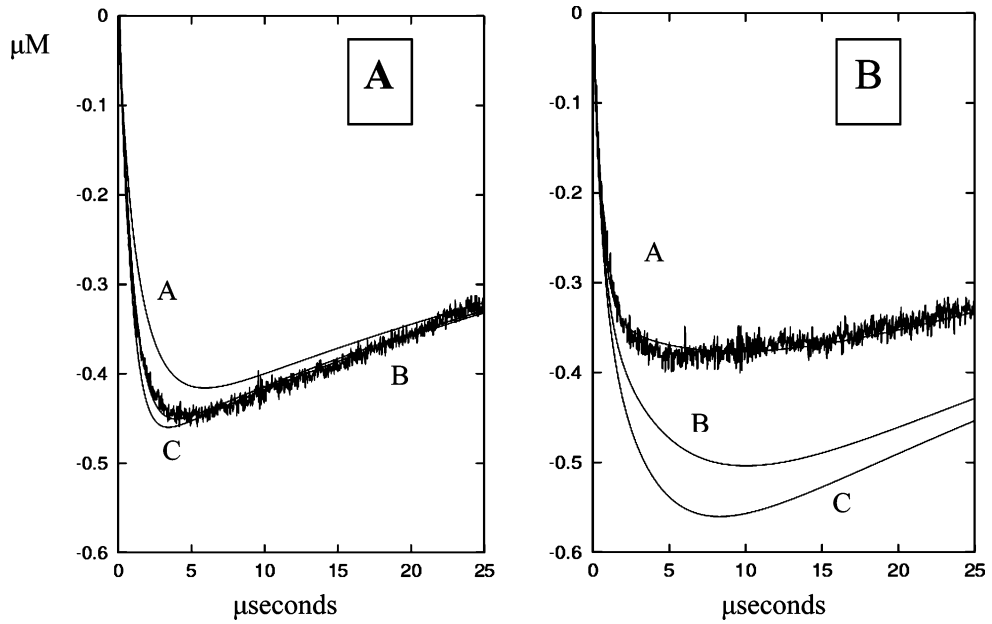

Figure 2. Reconstruction of the reversible protonation of fluorescein by numeric integration of the differential rate equations corresponding to the reactions defined by eqs 1−6, demonstrating the effect of the rate constant of reaction 6 on the dynamics. The ordinate denotes, in micromolar units, the amount of protonated fluorescein. The traces correspond with the experimental data presented in Figure 1, as measured at a higher time resolution. Frame A: The reaction was carried out in water, pH = 7.1, 20.8 °C. The three curves were reconstructed with the rate constants for reactions 1−5, as given in Table 1 (second column), except for that of the intramolecular reaction, which was varied with values of $k_6 = 5 \times 10^{10}$, 12.5×10^{10}, and 20×10^{10} for curves A, B, and C, respectively. Frame B: Reconstruction of the reaction as was carried out in D_2O, pH = 7.04, 22.8 °C. The three curves were reconstructed with the rate constants for reactions 1−5, as given in Table 1 (third column), except for that of the intramolecular reaction, which was varied with values of $k_6 = 0.2 \times 10^{10}$, 1.1×10^{10}, and 2×10^{10} for curves A, B, and C, respectively.

quent 20 ps long MD simulations were performed with the heavy atoms of the fluorescein and the hydronium oxygens restrained to their initial positions through force constants of 1000, 100, and 50 kJ mol^{-1} nm^{-1}, respectively. The force constants were then relaxed to 20 kJ mol^{-1} nm^{-1}, and the system was equilibrated for 50 ps before performing a 500 ps MD run. The position restraints were maintained to avoid the diffusion of the hydronium into the bulk water. It should be mentioned that this simulation was only used to compute the number of hydrogen bonds between the water and the hydronium when the latter is located in the vicinity of the dye, as proton-transfer events (or any events that involve the breaking or formation of

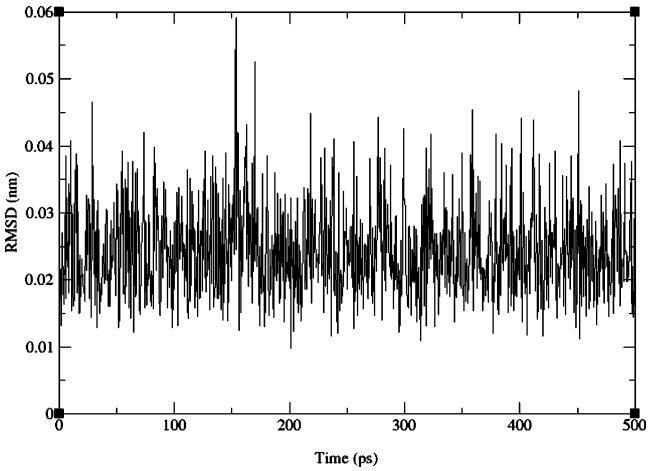

Figure 3. RMSD of all atoms in the fluorescein molecule during the molecular dynamics simulation. The all-atom RMSD is small and stable, indicating that the fluorescein is rigid during the MD simulation.

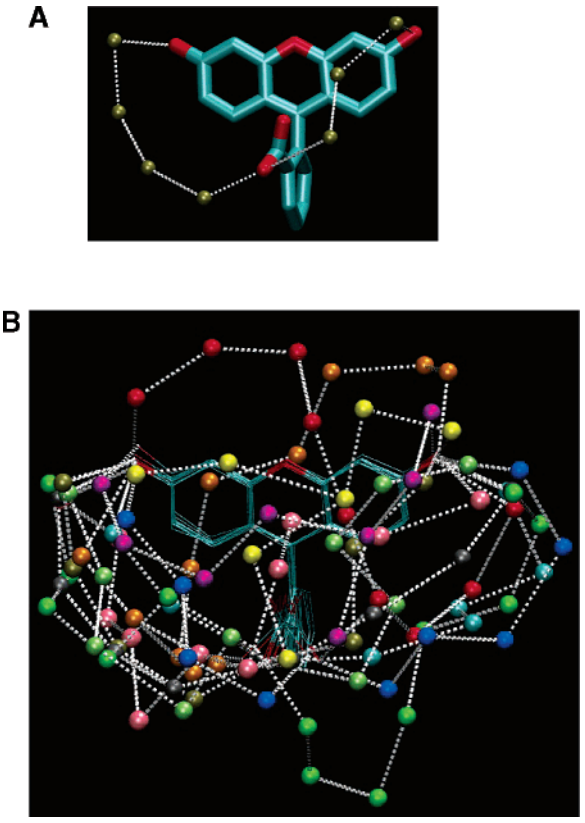

Figure 4. Array of water molecules that are at a hydrogen-bond distance and form a possible proton-conducting pathway between the protonated state of the carboxylate (donor) on the benzene ring of fluorescein and the proton acceptor oxygen atoms on the xanthene ring. Frame A depicts the shortest trajectories as found for two configurations, while, in Frame B, 10 trajectories are superpositioned. Frame B also exhibits the structural fluctuations of the dye's structure.

bonds) are not allowed to occur in classical MD simulations. Another simulation was performed where a hydronium ion was put into a box containing a similar number of water molecules (639) in order to compute the number of hydrogen bonds between the water and the hydronium when the latter is not located near the fluorescein molecule. A single Cl^- ion was added to neutralize the system's charge. The system was not subjected to any position restraints prior to the 500 ps MD run. Instead, it was gradually heated from 50 K to 250 K in 50 K steps during a period of 100 ps and was then equilibrated at 300 K for 50 ps. It should be stressed that the classical simulation was intended to approximate the effect of the solute molecule and its charges on the structure of the nearby water molecules. A precise description of the system necessitates quantum mechanical calculations which presently require a nonrealistic computation time. Both simulations were held under the same NPT conditions and used the same cutoffs and bond restraints as above. The H_3O^+ charges were calculated using HF with the 6-31G* basis set as described above for the fluorescein molecule.

Calculation and Representation of the Electrostatic Potential around the Fluorescein. The electrostatic potential around the fluorescein was calculated by solving the nonlinear Poisson−Boltzmann (PB) equation. The fluorescein anion was placed at the center of a cubic box with a length of 40 Å. The starting structure of the fluorescein molecule was modeled using the computer program GAMESS[45] and DFT with the 6-31G* basis set. The density functionals were calculated using the B3LYP functional.[47,48] The atomic charges were determined by fitting them to the electrostatic potential around the molecule using the Kollman−Singh method.[55] This approach complies with the setting of our MD simulations and was found to yield a relatively small error (1.39 kcal mol^{-1}) in the calculation of the hydration energies for a large set of organic molecules.[57] The atomic radii used to build the boundary between the solute and the solvent were 2.0 Å for the carbons, 1.55 Å for the oxygens, and 1.25 Å for the hydrogens, as used in ref 58. The solvent was represented as a continuum with a dielectric constant of $\epsilon = 78.4$. The dielectric constant of the solute was defined as $\epsilon = 2$. The nonlinear PB equation was solved by the computer program APBS[59] using a grid with a spacing of 0.312 Å. The potential was presented in Figure 6 using the computer program VMD.[60]

Results

Kinetic Measurements of the Intramolecular Proton Transfer. Figure 1A and B depicts the dynamics of proton transfer in a system consisting of a dilute aqueous solution of pyranine and fluorescein (~20 μM each). At $t = 0$, a laser pulse excited the photoacid molecule and caused proton ejection. The initial perturbation is too short to be resolved and appears as an instantaneous appearance of $\mathbf{\Phi O}^-$, as was measured at 458 nm (top curves). The relaxation of this signal corresponds with the reprotonation of the pyranine anion back to the prepulse level. The protonation of the fluorescein is recorded as a bleaching of the absorbance at 486 nm (bottom curves). In contrast to the pyranine signal, the protonation of the fluorescein has a well-resolved rise time, which corresponds with the protonation of the oxyanion of the chromophore ring structure.

The measurements were carried out either in H_2O (frame A) or in D_2O (frame B) and the experimental curves were reconstructed by numeric integration of the differential rate equations pertinent to reactions 1−6 (see above), using the reaction rate constants as adjustable parameters. The accuracy of the analysis is demonstrated in Figure 1, where the reconstructed curves are practically superpositioned over the experimental signals. The yielded rate constants, presented in Table 1, are the average of 10−15 reconstructions, each carried out for a signal measured under initial conditions that differed from the others.

The rate constants determined by the analysis for reactions 1−3 correspond with the diffusion-controlled reaction between a free proton and acceptor and are compatible with the values predicted by the Debye−Smoluchowski equation for diffusion-

TABLE 1: Rate Constants of Proton Transfer as Measured for the Pyranine−Fluorescein System in Water, in D_2O, and in 100 mM NaCl, All at 25 °C[a]

reaction	H_2O (M^{-1} s^{-1})	D_2O (M^{-1} s^{-1})	KIE	100 mM NaCl[b] (M^{-1} s^{-1})	E_a[c] (kcal mol^{-1}) in H_2O
$\mathbf{\Phi O^- + H^+}$	$9.2 \pm 0.14 \times 10^{10}$	$5.9 \pm 0.2 \times 10^{10}$	1.56	$5.6 \pm 0.2 \times 10^{10}$	3 ($R^2 = 0.775$)
$\mathbf{FLU^- + H^+}$	$2.5 \pm 0.25 \times 10^{10}$	$1.7 \pm 0.2 \times 10^{10}$	1.47	$1.6 \pm 0.2 \times 10^{10}$	3.3 ($R^2 = 0.645$)
$\mathbf{COO^- + H^+}$	$2.5 \pm 0.25 \times 10^{10}$	$1.7 \pm 0.2 \times 10^{10}$	1.47	$1.6 \pm 0.2 \times 10^{10}$	3.3 ($R^2 = 0.645$)
$\mathbf{FLUH + \Phi O^-}$	$5.33 \pm 1.25 \times 10^{8}$	$3.9 \pm 0.78 \times 10^{8}$	~1.3	$11.3 \pm 1.7 \times 10^{8}$	ND
$\mathbf{COOH + FLU^-}$	$\mathbf{23.3 \pm 2.5 \times 10^{10}}$	$\mathbf{0.43 \pm 0.08 \times 10^{10}}$	**54.2**	$\mathbf{6.5 \pm 0.5 \times 10^{10}}$	**11** ($R^2 = 0.691$)

[a] All rate constants are given in M^{-1} s^{-1}. The rate constants are defined in eqs 1−6. The values given in the table are means of the analysis of 15 independent measurements carried out under different initial conditions. The rate constants for reaction 5 were small and had a negligible contribution to the overall dynamics. For this reason, they are not included in the table. [b] The rate constants determined in the presence of 100 KCl or CsCl are essentially those measured with NaCl. [c] The number in parentheses denotes the linear correlation factor calculated for the Arrhenius plot.

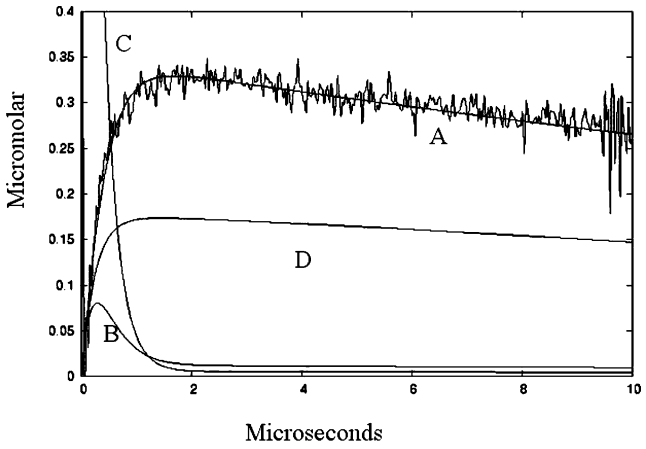

Figure 5. Reconstruction of the protonation dynamics of the fluorescein. The figure depicts the first 10 μs of the protonation of the fluorescein, under conditions similar to Figure 1A. Curve A represents the experimental signal with the superpositioned reconstruction. Curve B depicts the reversible protonation of the carboxylate residue of the dye. Curve C corresponds with the uptake of the free proton by the various proton acceptor sites present in the system (pyranine and the two sites of the dye). Please note that at $t = 0$ the free proton concentration is 2.4 μM. Curve D corresponds with the protonation dynamics of the fluorescein under hypothetical conditions where the intramolecular proton-transfer reaction is abolished and the protons released from the carboxylate have to diffuse into the bulk before they react with the chromophore.

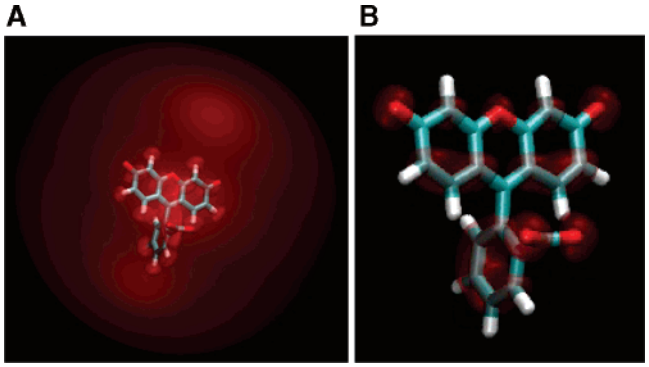

Figure 6. Electrostatic potential of the fluorescein dianion as calculated for $I = 0$ (A) or in the presence of screening electrolyte $I = 100$ mM (B). The red colored space shows where the negative potential is equal, or higher, than k_BT.

controlled reactions.[5,41−44] Reactions 4 and 5 describe a collisional proton transfer from each of the protonated sites of the fluorescein toward the more basic acceptor, the pyranine anion. These rate constants are also compatible with the theoretical predictions. Reaction 6 differs from these reactions, as it has an extremely fast rate constant that exceeds the Debye−Smoluchowski prediction by 2 orders of magnitude. The fluorescein molecule has a radius of ~6 Å and a diffusion coefficient of $\sim 1 \times 10^{-5}$ cm^2 s^{-1}, and it can bear either one or two negative charges. The proton transfer as pertinent to reaction 6 implies an encounter between two fluorescein molecules, one having a charge of −1 (protonated on the carboxylate moiety) and the other two negative charges. The expected rate constant, calculated by the Debye−Smoluchowski equation, is, at a vanishing ionic strength, as slow as $k \sim 3 \times 10^9$ M^{-1} s^{-1}. This value is smaller by 2 orders of magnitude than the measured rate constant of $\sim 2.3 \times 10^{11}$ M^{-1} s^{-1}, which negates a reaction mechanism based on encounter between two fluorescein molecules. Accordingly, the mechanism must be identified as an intramolecular proton transfer, where the proton is first released from the benzene's carboxylate and then preferentially reacts with the nearest proton-binding site, which is the chromophore's oxyanion. It should be stressed that the magnitude and the units of the reaction utilize second-order rate constant units. For these reasons, we shall use the calculated rate constant of the intramolecular proton transfer as an expression of the efficiency of the process, where high values imply that the pathway competes successfully with the other pathway, where the proton is dispersed into the bulk of the solution before re-encounter with the Coulomb cage of the fluorescein.

The inclusion of the intramolecular proton transfer is essential for the accurate reconstruction of the measured signals. The sensitivity of the calculated dynamics to the rate constant of the intramolecular reaction is demonstrated in Figure 2, which emphasizes the dynamics during the first 25 μs of the reaction, that is, the time frame where the intramolecular reaction dominates. It can be clearly seen that the magnitude of the intramolecular proton-transfer reaction, which fits best for the experimental curve, has a rate constant of $\sim 1.3 \times 10^{11}$ M^{-1} s^{-1}. This value is ~50 times larger than the expected rate of encounter between two fluorescein molecules in the solution. In the rest of this study, we shall focus on the intramolecular proton-transfer reaction and evaluate its mechanism.

Effect of Solvent on the Proton Transfer. *1. Kinetic Isotope Effect.* The kinetic measurements were repeated, using D_2O as the solvent, and the results are presented in Figures 1B and 2B. The difference in the dynamics, as recorded in the two solvents, is readily detected by visual inspection of the figures. The results of the kinetic analysis are presented in Table 1, column 3. The rate constants determined for the diffusion-controlled reactions between free proton and acceptor molecules were lower in D_2O, by a factor of KIE $\sim \sqrt{2}$, with respect to the values determined in water (rows 1−4 in Table 1). In contrast with these rate constants, the value assigned to the intramolecular reaction in D_2O was ~50 smaller than that in water, which is a tremendously large kinetic isotope effect. It must be stressed that, while a small deviation of the reconstructed curve from the measured one can be corrected by modulation of other rate constants, the

deviations presented in Figure 2 (frame A vs frame B) are too large to be corrected by any combination of all other rate constants. For this reason, the reduced rate constant for the intramolecular reaction, as measured in D_2O, is a true presentation of the reaction pathway.

2. Effect of Salt on the Proton Transfer. The passage of proton between the two proton-binding sites on the fluorescein molecule is very sensitive to the ionic screening. Repetition of the measurements in the presence of 100 mM screening electrolyte (NaCl, KCl, and CsCl) yielded a consistent set of rate constants (suitable for a reconstruction of approximately 10 independent measurements in the presence of each of the electrolytes), which are given in column 5 of Table 1. It should be noted that the collisional proton transfer between the fluorescein and the pyranine anions (reaction 4, row 4 in Table 1) is accelerated in the presence of the screening electrolyte. The addition of a screening electrolyte modified the rate of the diffusion-controlled reactions in accordance with the Debye−Smoluchowski equation, slowing the reactions between attractive reactants by ∼35% (rows 1, 2, and 3) and doubling the rate of reactions between repulsive reactants (row 4). The intramolecular proton-transfer process was much more sensitive to the ionic screening effect, which reduced the rate constant by a factor of ∼4. However, the rate constant of the intramolecular reaction is still faster by a factor of ∼10 than the upper limit of the Debye−Smoluchowski equation in a fully screened electrolyte solution.

3. Activation Energy of the Proton-Transfer Reactions. The interpretation of the high kinetic isotope effect measured for the intramolecular proton transfer necessitated measurement of the activation energy of the pathway. The proton-transfer kinetics, as presented in Figure 1, were repeatedly measured within a temperature range of 10 to 40 °C. The signals were analyzed, and the calculated activation energies are tabulated in Table 1, column 6. The activation energies that were measured for the diffusion-controlled reactions (k_1, k_3, and k_5) have values compatible with the variation of the water's viscosity with temperature ($E_a = 3-4$ kcal mol^{-1}) or of the proton's limiting equivalent conductivity (2.2 kcal mol^{-1}).[61] In contrast, the activation energy for the intramolecular process is significantly larger (11 kcal mol^{-1}). Thus, the mechanism that controls the intramolecular process exhibits a large kinetic isotope effect and also a large activation energy.

Measuring the activation energy in D_2O was experimentally impractical. In D_2O, the rate constant of the intramolecular reaction is already comparable with the diffusion-controlled limit of the Debye−Smoluchowski equation, which renders it to be practically undetectable. Thus, repetition of the dynamics in D_2O at varying temperatures yielded values that were too small and too erratic to have any mechanistic significance.

Modeling of Connectivity between the Carboxylate and the Oxyanion. The high activation energy and the large kinetic isotope effect values assigned to the intramolecular proton transfer are characteristic for proton transfer through a hydrogen bond that is slightly stretched beyond its equilibrium length.[17,18] Accordingly, we investigated whether the solute molecule, the fluorescein, may affect the water molecules in its immediate vicinity, searching for the presence of hydrogen-bonded water molecules that may serve as pathways through which the proton can propagate from the carboxylate to the oxyanion.

For a study of the fluorescein−water interactions, we used the fluorescein molecule with a single proton attached to the carboxylate moiety and carried out a 500 ps molecular dynamics simulation in the presence of 639 water molecules and one Na^+ as a counterion (see Methods for details). The simulation indicated that the fluorescein molecule is a rather rigid structure. The benzene ring exhibited only minor rotational fluctuations with respect to the chromophore, while the chromophore executed a minor flipping motion of rings 1 and 3 of the xanthene structure. The all-atoms RMSD is presented in Figure 3, while the nature of the structural fluctuations can be seen in frame B of Figure 4.

The protonated carboxyl moiety of the fluorescein was hydrogen-bonded with water for 95% of the simulation time, with an average of five hydrogen bonds. The acceptor oxygen atoms, attached to the xanthene rings, were permanently hydrogen-bonded with the water, averaging four hydrogen bonds. The hydrogen bonds between the dye and the water had a lifetime that was ∼2 times longer (5.80 and 5.13 ps for the carboxylate and the chromophore, respectively) than the average for hydrogen bonds between water molecules in the bulk (2.94 ps).

In the presence of so many water molecules, the proton can propagate from the donor to the acceptor by more than one trajectory. What is more, once the proton dissociates from the carboxylic moiety, it will affect the local structure of the water, by forming either $H_9O_4^+$ or $H_5O_2^+$ species. We limited the search to the water molecules in the vicinity of the dye for molecules that are at a suitable distance to form a hydrogen-bonded array, using the default value of the GROMACS program $r \leq 3.5$ Å. The search was aimed to find the shortest pathway, and no attempt was made to find whether, at a given set of coordinates, there is more than one pathway with the same number of interconnecting water molecules. The search was carried out with respect to the two oxyanions of the chromophore. An example of such trajectories is presented in Figure 4A, while 10 superpositioned trajectories are in frame B.

As seen in these figures, the connecting pathways can vary in length and shape. The shortest one consists of two water molecules, while, in some transient fluorescein−water configurations, the connection was much longer. On average, four to five water molecules sufficed to establish the connectivity between donor and acceptor sites. To obtain a more realistic presentation, frame B is a superposition of 10 trajectories. Examination of this figure indicates that the connectivity is established by a section of the space surrounding the dye molecule. The connection of the two sites by the water molecules is a flexible yet persistent feature. The length of the path varies with time, even within a 1 ps time frame, and so does the shape of the path. However, in all cases, the path remained close to the surface of the molecule and did not extend out of the Coulomb cage of the molecule (see Figure 6A).

Discussion

In the present study, we investigated the mechanism of proton transfer between two sites fixed on a small, well solvated molecule, that was taken as a model for proton transfer between adjacent sites on a protein. The results indicated that the reaction proceeds through a mechanism that is characterized by a large kinetic isotope effect, high activation energy, and sensitivity to ionic screening. The reaction under study is a proton transfer between adjacent sites: a carboxylate and oxyanion located some 6 Å apart on the fluorescein molecule. The measurements were carried out under experimental conditions which ensured that only one proton could react with the dye, and the low concentrations of the reactants ensured that the rate-limiting step of the protonation was the encounter of the free proton with the Coulomb cage of the double ionized dye. For a molecule with a total charge of $Z = -2$ dissolved in water, the Coulomb cage at vanishing ionic strength has a radius of 14 Å (see Figure

6). Once the proton penetrated the Coulomb cage, its random walk was strongly biased by the local electrostatic potential and it could form a covalent bond with either of the proton-binding sites in less than a nanosecond.[62] There are two nonidentical products of this reaction. The first is the protonated state of the chromophore's oxyanion. This is a rather stable product (pK = 6.6), characterized by a distinct spectral shift. The intrinsic dissociation time of this product ($\tau \sim 0.16$ ms) is comparable with the experimental observation time. As the observed decay is significantly shorter (see Figure 1), most of the deprotonation of this species takes place through collisional proton transfer with the strongest base in the system, the pyranine anion. The second product of the encounter between the free proton and the dye is the protonated state of the benzene's carboxylate. This is a spectrally silent species, having pK = 5.2 and an intrinsic dissociation time constant of $\sim 3\ \mu$s. Consequently, its major relaxation pathway will be spontaneous proton diffusion rather than a collisional reaction. The proton released from the carboxylate can either diffuse to the bulk or react with the proton-binding sites present inside the Coulomb cage. The dispersive pathway is retarded by the confining electrostatic potential. The escape time from a Coulomb cage with a radius of 14 Å, as in the case of fluorescein, had been calculated to be $\tau \sim 0.6$ ns.[42] During the time when the proton is attempting to diffuse out of the cage, it has ample opportunity to react with one of the oxyanions of the chromophore, forming the more stable protonated chromophore. This event is detected by the analysis as a parallel pathway that contributes to the protonation of the oxyanion, which can be visualized by the simulation procedure. Curve A in Figure 5 represents the experimental signal of fluorescein protonation as recorded during the first 25 μs of the kinetics. On top of the experimental data, we present the reconstructed dynamics generated by the rate constants in Table 1. The protonation of the chromophore is a fast reaction, which reached its maximum within less than 2 μs. In parallel with the protonation of the chromophore, there is an accumulation of the protonated state of the benzene's carboxylate (Figure 5, curve B). However, unlike the oxyanion, the carboxylate loses its proton within the first 2 μs. This deprotonation proceeds within the time frame where the free proton concentration in the solution exceeds the prepulse level (curve C), indicating that the carboxylate transfers its proton to an acceptor through a pathway that is faster than the rate at which free proton can react with the oxyanion. Repetition of the simulation under hypothetical conditions, where the intramolecular reaction is not operative (i.e., the rate constants of reaction 6 are set to zero), reduced the yield of the protonated chromophore by half (curve D). This simulation demonstrates how efficient a proton transfer can be between consenting sites sharing the same Coulomb cage.

The dynamics of proton dissociation inside the Coulomb cage are best described by the geminate recombination formalism of Agmon,[63] which states that, as long as the proton is located within the cage, its probability to re-encounter the parent molecule is higher than that of a proton in the bulk. The intensive electrostatic field inside the cage, and its small dimension, render the propagation and encounter events inside the cage to be in the sub-nanosecond time range. Naturally, such fast reactions are unobserved when the reaction is initiated by proton in the bulk, for which the rate-limiting step is the encounter of the proton with the outer perimeter of the Coulomb cage. Thus, the common kinetic terms k_{dis} and k_{as}, which quantitate the appearance and consumption of the free proton at the perimeter of the Coulomb cage, are not sufficiently adequate to describe reactions inside the Coulomb cage. Inside the cage, the dissociation event is expressed by the term κ_f. This is the rate constant at which the proton is transferred from the acidic moiety to nearby water molecules that, through solvation, overcome the intensive electrostatic attraction between the charge of the proton and the anionic state of the parent molecule. The reverse reaction, where the solvated proton reacts with the anion to form the acid state, takes place at the surface of the reaction sphere, and its rate constant is given by κ_r.[64] The standard kinetic terms k_{dis} and k_{as} are related to κ_f and κ_r through expressions that combine the dynamics at the surface of the reaction sphere, the radius of the cage, and the diffusion coefficient of the proton.[63] Since a proton released from the acidic moiety can recombine a few times with the parent molecule before it diffuses out of the Coulomb cage, the value of κ_f is 1.5−2-fold larger than k_{dis} (for details, see ref 63). The pacemaker of the intra-Coulomb cage proton transfer is the primary dissociation of the proton from the carboxylate.

The model used for the simulation of a free proton inside the Coulomb cage, the geminate recombination model of Agmon,[63] is based on the continuum approximation, where the proton is a point charge that moves in a structureless matrix. This presentation does not have the capability to explain the peculiar features such as the KIE, activation energy, and the effect of ionic screening on the intramolecular proton transfer, and a more detailed description that accounts for water at a molecular detail is needed. The diffusion of the solvated proton in water follows a complex mechanism, where the two stable configurations $H_9O_4^+$ and $H_5O_2^+$ are in rapid equilibrium affected by the random motion of the water molecules in the solvation shell of the two charged species.[6,8−11,65−67] Both species are interchangeable through the motion of the proton, along the proton coordinate, whenever the random motions of the solvent set up a situation that enables the proton to move from the donor's potential well to that of the acceptor along an equipotential trajectory. The energy barrier that the proton has to overcome is rather low, in the order of $\sim k_B T$,[10] and is significantly smaller than the experimental value 2.5 kcal mol^{-1}, that is equated with the reorganization energy.[68] The activation energy we had measured for the proton transfer from the carboxylate to the oxyanion is much larger, indicating that the mechanism of this proton transfer differs from the reaction in bulk water. In the same sense, the kinetic isotope effect of proton transfer that had been measured is larger than the reaction in the bulk, that is, $\sim\sqrt{2}$.[11] In the following discussion, we shall attempt to account for our observations in terms of the proton transfer through the water molecules that make the inner solvation shell of the fluorescein molecule.

The water molecules in the immediate vicinity of the fluorescein were subjected to molecular dynamics simulation. The results of these calculations, as presented in Figure 4, demonstrate that the carboxylate and the oxyanion are hydrogen-bonded through a few water molecules. The average lifetime of these bonds is about twice as long as those of bulk water, indicating that the dye reorders the water in its first solvation shell. Molecular dynamics that were carried out with a hydronium next to the dye revealed that the combination of the negative sites and the positive charge of the proton extended the lifetime of the hydrogen bonds to $\tau = 15.18$ ps, which is twice the $\tau = 8.63$ ps as calculated for hydronium in bulk water. The gained stability of the hydrogen bond in the immediate vicinity of the dye, supported by the high sensitivity of the intramolecular to ionic screening, indicates that the water inside the Coulomb cage differs from bulk water in its capacity to participate in proton transfer. These conclusions, based on

molecular dynamics, are supported by the results of Kropman and Bakker.[69,70] In these measurements, an intense mid-infrared pump pulse was used to excite HDO molecules to the first excited state of the O−H vibration. The relaxation of the system led to stochastic changes in the O−H···A hydrogen-bond lengths, where A is either water oxygen (when the measurements were carried out in neat water) or halogen ion (when the measurements were carried out in solutions of alkali-halogen salts). It was shown that the correlation time constant τ_c of the stochastic modulation of the O−H···Y^- hydrogen-bond length (Y^- stands for a halogen anion) was 25−50 times longer than τ_c for O−H···O hydrogen bonds. The difference was attributed to the relatively long-living, well-defined structure formed by the aqueous solvation shell around the anions.

The order imposed by the fluorescein on the inner solvation layer may account for the special features of the intramolecular proton-transfer reactions. The proton transfer between two water molecules is regulated by the motion of the water molecules in the whole structure of the solvated proton; the hydrogen bonds in the second and third layer are rearranged, destabilizing bonds are broken, and stabilizing bonds are formed. During the passage of the protonic charge, the hydrogen bonds are temporarily constricted.[8] These local rearrangements of structure are hampered by the structure imposed by the negative charges of the anion, forcing the proton transfer to take place in a more rigid environment where the O−O distances are larger than 2.4 Å. As a result, both the activation energy and the kinetic isotope effect increase. Scheiner and co-workers[16,17] have investigated the effect of the interatomic distance on the activation energy and the KIE of proton transfer. These quantum mechanical calculations show that the energy barrier for proton transfer increases with the distance between the oxygen atoms of the water, reaching a value of 15−20 kcal mol^{-1} at a separation of ~2.8 Å.[16,17] Furthermore, under these conditions, the proton transfer operates both by a classical mechanism (transition state theory) and by tunneling, thus leading under certain conditions to a very high kinetic isotope effect.[18] In bulk water, the length of the hydrogen bond in the Eigen or the Zundel structures is in the order of 2.4 Å and the measured activation energy represents the reorganization of the solvent.[8] However, when the water molecules are held by the ordering forces of the charged scaffolding, the reaction operates under a different regime, where the concerted motion of the water molecule, as required to facilitate the proton transfer, is restricted and the rate-limiting step is shifted from the organization of the solvent to the passage of the proton, with subsequent enhancement of the activation energy and kinetic isotope effect.

A question to be answered is why the proton remains in the vicinity of the acceptor water molecule (which is part of the interconnecting trajectory, as in Figure 4B) instead of escaping to the bulk. This can be explained by the presence of the intensive electrostatic potential that detains the proton within the space defined by the Coulomb cage. The diffusion out of the Coulomb cage is an uphill diffusion with an escape time in the order of hundreds of picoseconds,[42] while the intramolecular reaction hardly overcomes an electrostatic barrier. Thus, while the released proton is attempting to diffuse out of the Coulomb cage, there is ample opportunity to propagate through the rigidified water molecules.

The collapse of the local electrostatic potential by high concentrations of electrolyte is consistent with our interpretation. In the presence of 100 mM NaCl, the ionic screening practically abolishes the wrapping Coulomb cage (see Figure 6B). In the absence of the retarding potential, the proton can readily disperse to the bulk and the intramolecular reaction is slowed, to a level that reflects the proximity of the acceptor site to the site of release.

At present, our kinetic measurements revealed the major contribution of proton transfer between sites located inside a common Coulomb cage on the dynamics of proton transfer. Further support will come from a new kind of measurements, carried out in the sub-nanosecond time frame, where a proton acceptor will be positioned next to a photoacid so that its contribution to the observations can be directly measured and reconstructed by the geminate recombination formalism. In parallel, advanced molecular dynamics simulations, which incorporate quantum mechanical terms, and the subsequent analysis of possible proton tunneling events, should be carried out in order to provide detailed mechanistic support for the observations.

Concluding Remarks

The present study documents that proton transfer between nearby sites, which are located on a rigid scaffolding, employs a pathway that utilizes the ordered water in the first solvation layer as a carrier. This mechanism can offer an efficient mechanism by which protons are transferred between sites with little loss to the bulk. Such a mechanism has a physiological advantage under conditions where an enzyme has to react with free proton at pH > 7 values where the free proton concentration is very low.

The explanation derived for the mechanism is based on quantum mechanical calculations which, at present, are limited to simple model molecules in vacuo. Indeed, the classical molecular dynamics substantiate our conclusions, yet the corroboration of the model necessitates reopening of the case and modeling of both the fluorescein and the surrounding water by ab initio or equivalent computation methods suitable for reproducing the proton-transfer events.[71−73] Such calculations and further time-resolved measurements are presently under study.

Acknowledgment. The authors are grateful to Professor Steve Scheiner, from Utah State University, for his assistance and advice. The research in the Laser Laboratory for Fast Reactions in Biology is supported by the following research grants: The Israeli Science Foundation (472/01-2), the German-Israeli Foundation for Scientific Research and Development (G.I.F) (I−140-207.98), and the American Israel Bi-national Science Foundation (2002129). R.F. would like to acknowledge the Colton Foundation for a Colton Fellowship. The authors would also like to acknowledge the use of computer resources which belong to the Bioinformatics Unit at Tel Aviv University and the High Performance Computing Unit, a division of the Inter University Computing Center, which is a consortium formed by research universities in Israel.

Supporting Information Available: The charges and atom types used in the MD simulation of fluorescein. This material is available free of charge via the Internet at http://pubs.acs.org.

References and Notes

(1) Adelroth, P.; Sigurdson, H.; Hallen, S.; Brzezinski, P. *Proc. Natl. Acad. Sci. U.S.A.* **1996**, *93*, 12292.

(2) Adelroth, P.; Mitchell, D. M.; Gennis, R. B.; Brzezinski, P. *Biochemistry* **1997**, *36*, 11787.

(3) Adelroth, P.; Ek, M. S.; Mitchell, D. M.; Gennis, R. B.; Brzezinski, P. *Biochemistry* **1997**, *36*, 13824.

(4) Checover, S.; Marantz, Y.; Nachliel, E.; Gutman, M.; Pfeiffer, M.; Tittor, J.; Oesterhelt, D.; Dencher, N. A. *Biochemistry* **2001**, *40*, 4281.

(5) Gutman, M.; Nachliel, E. *Annu. Rev. Phys. Chem.* **1997**, *48*, 329.
(6) Agmon, N. *Isr. J. Chem.* **2000**, *39*.
(7) Kuznetsov, A. M.; Ulstrup, J. *Chem. Phys.* **1994**, *188*, 131.
(8) Lapid, H.; Agmon, N.; Petersen, M. K.; Voth, G. A. *J. Chem. Phys* **2005**, *122*, 14506.
(9) Agmon, N. *Chem. Phys. Lett.* **1995**, *244*, 456.
(10) Marx, D.; Tuckerman, M. E.; Hutter, J.; Parrinello, M. *Nature* **1999**, *397*, 601.
(11) Kornyshev, A. A.; Kuznetsov, A. M.; Spohr, E.; Ulstrup, J. *J. Phys. Chem. B* **2003**, *107*, 3351.
(12) Tuckerman, M. E.; Marx, D.; Parrinello, M. *Nature* **2002**, *417*, 925.
(13) Krishtalik, L. I. *Biochim. Biophys. Acta* **2000**, *1458*, 6.
(14) Scheiner, S. *Biochim. Biophys. Acta* **2000**, *1458*, 28.
(15) Scheiner, S. *Ann. N.Y. Acad. Sci.* **1981**, *367*, 493.
(16) Scheiner, S. *J. Am. Chem. Soc.* **1981**, *103*, 315.
(17) Hillenbrand, E. A.; Scheiner, S. *J. Am. Chem. Soc.* **1984**, *106*, 6266.
(18) Scheiner, S.; Latajka, Z. *J. Phys. Chem.* **1987**, *91*, 724.
(19) Agmon, N.; Huppert, D.; Massad, A.; Pines, E. *J. Phys. Chem.* **1991**, *95*, 666.
(20) Barone, V.; Adamo, C. *J. Comput. Chem.* **1994**, *15*, 395.
(21) Brauer, M.; Mosquera, M.; Perez-Lustres, J. L.; Rodriguez-Prieto, F. *J. Phys. Chem.* **1998**, *102*, 10736.
(22) Carballeira, L.; Perez-Juste, I. *J. Mol. Struct.* **1996**, *368*, 17.
(23) Cleland, W. W. *Arch. Biochem. Biophys.* **2000**, *382*, 1.
(24) Fores, M.; Duran, M.; Sola, M. *Chem. Phys.* **1998**, *234*, 1.
(25) Guharay, J.; Dennison, S. M.; Sengupta, P. K. *Spectrochim. Acta* **1999**, *55A*, 1091.
(26) Gutman, M.; Huppert, D.; Nachliel, E. *Eur. J. Biochem.* **1982**, *121*, 637.
(27) Gutman, M.; Nachliel, E.; Huppert, D. *Eur. J. Biochem.* **1982**, *125*, 175.
(28) Htun, T. M.; Suwaiyan, A.; Klein, U. K. A. *Chem. Phys. Lett.* **1995**, *243*, 71.
(29) Liedl, K. R.; Sekusak, S.; Kroemer, T.; Rode, B. M. *J. Phys. Chem. A* **1997**, *101*, 4707.
(30) Lima, J. C.; Abreu, I.; Brouillard, R.; Macanita, A. L. *Chem. Phys. Lett.* **1998**, *298*, 189.
(31) Masad, A.; Huppert, D. *J. Phys. Chem.* **1992**, *96*, 7324.
(32) Rini, M.; Magnes, B. Z.; Pines, E.; Nibbering, E. T. *Science* **2003**, *301*, 349.
(33) Tran-Thi, T. H.; Gustavsson, T.; Prayer, C.; Pommeret, S.; Hynes, J. T. *Chem. Phys. Lett.* **2000**, *329*, 421.
(34) Michel, H. *Nature* **1999**, *402*, 602.
(35) Folmer, D. E.; Wisniewski, E. S.; Castleman, A. W., Jr. *Chem. Phys. Lett.* **2000**, *318*, 637.
(36) Gutman, M. *Methods Biochem. Anal.* **1984**, *30*, 1.
(37) Gutman, M. *Methods Enzymol.* **1986**, *127*, 522.
(38) Yam, R.; Nachliel, E.; Gutman, M. *J. Am. Chem. Soc.* **1988**, *110*, 2636.
(39) Gutman, M.; Nachliel, E. *Biochemistry* **1985**, *24*, 2941.
(40) Gutman, M.; Nachliel, E.; Gershon, E. *Biochemistry* **1985**, *24*, 2937.
(41) Gutman, M.; Nachliel, E. *Biochim. Biophys. Acta* **1990**, *1015*, 391.
(42) Gutman, M.; Nachliel, E. *Biochim. Biophys. Acta* **1995**, *1231*, 123.
(43) Nachliel, E.; Gutman, M. *Biochem. Biophys. Acta* **2001**, *1514*, 50.
(44) Nachliel, E.; Gutman, M.; Tittor, J.; Oesterhelt, D. *Biophys. J.* **2002**, *83*, 416.
(45) Schmidt, M. W.; Baldridge, K. K.; Boatz, J. A.; Elbert, S. T.; Gordon, M. S.; Jensen, J. J.; Koseki, S.; Matsunaga, N.; Nguyen, K. A.; Su, S.; Windus, T. L.; Dupuis, M.; Montgomery, J. A. *J. Comput. Chem.* **1993**, *14*, 1347.
(46) Becke, A. *J. Chem. Phys.* **1993**, *98*, 1372.
(47) Becke, A. *J. Chem. Phys.* **1993**, *98*, 5648.
(48) Lee, C.; Yang, W.; Parr, R. G. *Phys. Rev. B* **1988**, *37*, 785−789.
(49) Jorgensen, W. L.; Chandrasekhar, J.; Madura, J. D.; Impey, R. W.; Klein, M. L. *J. Chem. Phys.* **1983**, *79*, 926.
(50) Lindahl, E.; Hess, B.; van der Spoel, D. *J. Mol. Model.* **2001**, *7*, 306.
(51) Jorgensen, W. L.; Severance, D. L. *J. Am. Chem. Soc.* **1990**, *112*, 4768.
(52) Chandrasekhar, J.; Spellmeyer, D. C.; Jorgensen, W. L. *J. Am. Chem. Soc.* **1984**, *106*, 903.
(53) Jorgensen, W. L.; McDonald, N. A. *THEOCHEM* **1998**, *424*, 145.
(54) Jorgensen, W. L.; Maxwell, D. S.; Tirado-Rives, J. *J. Am. Chem. Soc.* **1996**, *118*, 11225.
(55) Singh, U. C.; Kollman, P. A. *J. Comput. Chem.* **1984**, *5*, 129.
(56) van Aalten, D. M. F.; Bywater, R.; Findlay, J. B. C.; Hendlich, M.; W., H. R. W.; Vriend, G. *J. Comput.-Aided Mol. Des.* **1996**, *10*, 255.
(57) Green, D. F.; Tidor, B. *J. Phys. Chem. B* **2003**, *107*, 10261.
(58) Jang, Y. H.; Hwang, S.; Chung, D. S. *Chem. Lett.* **2001**, *30*, 1316.
(59) Baker, N. A.; Sept, D.; Joseph, S.; Holst, M. J.; McCammon, J. A. *Proc. Natl. Acad. Sci. U.S.A.* **2001**, *98*, 10037.
(60) Humphrey, W.; Dalke, A.; Schulten, K. *J. Mol. Graphics* **1996**, *14*, 33.
(61) Robinson, R. A.; Stokes, R. H. *Electrolyte solutions*; Butterworth: London, 1959.
(62) Forster, T. H.; Volker, S. *Chem. Phys. Lett.* **1975**, *34*, 1.
(63) Pines, E.; Huppert, D.; Agmon, N. *J. Chem. Phys.* **1988**, *88*, 5620.
(64) Cohen, B.; Huppert, D.; Solntsev, K. M.; Tsfadia, Y.; Nachliel, E.; Gutman, M. *J. Am. Chem. Soc.* **2002**, *124*, 7539.
(65) Walbran, S.; Kornyshev, A. A. *J. Chem. Phys.* **2001**, *114*, 10039.
(66) Ando, K.; Hynes, J. T. *J. Mol. Liq.* **1995**, *64*, 25.
(67) Marx, D.; Tuckerman, M. E.; Parrinello, M. *J. Phys: Condens. Matter* **2000**, *12*, A153.
(68) Kornyshev, A. A.; Kuznetsov, A. M.; Stimming, U. *J. Chem. Phys.* **1997**, *106*, 9523.
(69) Kropman, M. F.; Bakker, H. J. *J. Chem. Phys.* **2001**, *115*, 8942.
(70) Kropman, M. F.; Nienhuys, H. K.; Woutersen, S.; Bakker, H. J. *J. Phys. Chem. A* **2001**, *105*, 4622.
(71) Car, R.; Parrinello, M. *Phys. Rev. Lett.* **1985**, *55*, 2471.
(72) Ilan, B.; Tajkhorshid, E.; Schulten, K.; Voth, G. A. *Proteins* **2004**, *55*, 223.
(73) de Groot, B. L.; Frigato, T.; Helms, V.; Grubmuller, H. *J. Mol. Biol.* **2003**, *333*, 279.